Nanoscale

PAPER

View Article Online
View Journal | View Issue

Cite this: *Nanoscale*, 2021, **13**, 14139

Improving performance of luminescent nanothermometers based on non-thermally and thermally coupled levels of lanthanides by modulating laser power†

Natalia Stopikowska, Marcin Runowski,* Małgorzata Skwierczyńska and Stefan Lis

This work sheds light on the pump power impact on the performance of luminescent thermometers, which is often underestimated by researchers. An up-converting, inorganic nanoluminophore, YVO_4:Yb^{3+}, Er^{3+} (nanothermometer) was synthesized using the hydrothermal method and a subsequent calcination. This nanomaterial appears as a white powder composed of small nanoparticles (≈20 nm), exhibiting a very intense, green upconverted luminescence (λ_{ex} = 975 nm), visible to the naked eye. Its emission spectrum consists of four Er^{3+} bands (500–850 nm) and one Yb^{3+} band (>900 nm). The obtained compound exhibits temperature-dependent luminescence properties, hence it is used as an optical nanosensor of temperature. The determined band intensity ratios of the non-thermally coupled levels (non-TCLs) of Yb^{3+}/Er^{3+} and thermally coupled levels (TCLs) of Er^{3+} are correlated with temperature, and they are used for ratiometric sensing of temperature. The effects of the pump (NIR laser) power on the luminescence properties of the material, including band intensity ratios, absolute and relative sensitivities and temperature resolution are analysed. It was pointed out that the applied laser power has a huge impact on the values of the aforementioned thermometric parameters, and manipulating the laser power can significantly improve the performance of optical nanothermometers.

Received 3rd March 2021,
Accepted 19th July 2021

DOI: 10.1039/d1nr01395e

rsc.li/nanoscale

Introduction

The most commonly developed luminescent sensors of temperature are based on lanthanide (Ln) ions, such as Yb^{3+}, Er^{3+}, Tm^{3+}, Ho^{3+} and Nd^{3+} embedded in various matrices (*e.g.* Gd_2O_3, Al_2O_3, YF_3, YVO_4 and $NaYF_4$).[1–9] These ions exhibit unique luminescence properties, *i.e.* long luminescence lifetimes, narrow emission bands, multi-range emission, as well as the possibility of various energy migration processes between co-dopant ions.[10–14]

The systems based on up-conversion (two-photon) luminescence are particularly attractive from the point of view of biological research. They enable excitation of the material in the NIR range of the 1st (650–950 nm) or 2nd (1000–1350 nm) biological window (*e.g.* by Yb^{3+} excitation),[1] and detection of emissions in the 1st biological window (*e.g.* emission of Er^{3+}, Tm^{3+}, Ho^{3+} or Nd^{3+}).[1–4,9,11,12,15–19] Emission and excitation in the biological window ranges result in less absorption and scattering of light by tissues such as skin and blood.[1,15,16,18,20–22] In contrast, using conventional luminescence, where excitation often takes place in the UV or visible spectral range, a significant part of the radiation may be absorbed/scattered by the surrounding medium, diminishing excitation effectiveness of the ions embedded into the structure of such nanothermometers.[5,20] However, for temperature nanosensors used in other applications, *e.g.* in catalysis and optoelectronics, alike excitation and emission can take place over the entire spectral range.[23–25]

Optical sensors based on Ln ions usually enable temperature control based on the analysis of changes in the intensity ratios of the bands associated with their thermally and non-thermally coupled levels (TCLs and non-TCLs). In the case of two thermalized levels, where the energy of these levels does not differ too much (up to ≈2000 cm^{-1}), due to additional thermal energy, the photon may move from the level with lower energy to the level with higher energy. This will result in a decrease in the intensity of the lower energy band and the

Adam Mickiewicz University, Faculty of Chemistry, Department of Rare Earths, Uniwersytetu Poznańskiego 8, 61-614 Poznań, Poland. E-mail: runowski@amu.edu.pl ; Tel: +48618291778

†Electronic supplementary information (ESI) available: Transmission data for the optical filter used; normalized emission spectra measured at increasing temperature; non-normalized emission spectra measured at increasing temperature; integrated luminescence intensities as a function of temperature; log–log dependence of the luminescence intensity on the laser power; and thermal cycling experiments. See DOI: 10.1039/d1nr01395e

appearance (or increase in the intensity) of a higher energy band in the emission spectrum.[13,20,22,26,27] The Boltzmann type sensors based on the thermalized levels are already well-known, as they have been extensively investigated in the last decade.[12,14,28–30] However, there are some recent reports on deviations from the Boltzmann distribution in TCLs, which are concentration- or temperature-dependent.[31,32] On the other hand, luminescent thermometers based on non-TCLs, which take advantages of temperature-dependent rates of quenching/energy transfer, are also becoming more and more popular.[8,20,33–35] It is worth noting that temperature influences the spectroscopic properties of Ln ions such as: shortening of emission lifetimes, bandwidths (band broadening), changes in luminescence intensity ratios, and so forth.[12,13,16,19,26,29,32,34] Such temperature-dependent properties can be further used for thermal sensing purposes.

The optimal nanothermometer should show a high relative sensitivity and good temperature resolution.[8,12,20,36] It should be emphasized that the relative sensitivity of the luminescent thermometers operating with TCLs is intrinsically limited with the energy difference between these TCLs.[21,34,35] These limitations can be overcome by operating with non-TCLs of the optically active ions. Sensors showing the best performance can be successfully used in biological, electronic, engineering and other industrial processes to control the temperature of the system, *e.g.* the rate of catalytic processes or the progress of the polymerization process.[1,18,20,23–25,37]

Here we report the development of a ratiometric, optical nanothermometer, YVO_4:Yb^{3+},Er^{3+} working in a broad spectral range (VIS-NIR). The nanomaterial synthesized shows green up-conversion luminescence visible to the naked eye, and good temperature response (temperature-dependent luminescence). The selected luminescence intensity ratios of the bands associated with TCLs and non-TCLs of Er^{3+} and Yb^{3+} are used as thermometric parameters. The corresponding absolute and relative sensitivities, and temperature resolutions are investigated. A very important and novel aspect of this work is the demonstration of a strong influence of the applied pump (laser) power on the values of the mentioned thermometric parameters, as well as on the thermometer performance.

Experimental

Materials

RE_2O_3 (RE = Y^{3+}, Yb^{3+} and Er^{3+}) (99.99%, Stanford Materials) were separately dissolved in HCl (35–38%, pure P.A. – basic, POCh. S.A.) to obtain the corresponding chlorides $RECl_3$, and then evaporated to remove the excess acid. The following reagents were purchased from Sigma-Aldrich: ammonium metavanadate (ACS reagent, ≥99.0%) and PEG 6000. Sodium hydroxide (98.8% pure P.A.) was purchased from POCh. S.A. Deionized water was used for all experiments.

Synthesis of YVO_4:Yb^{3+},Er^{3+}

To synthesize 0.5 g of the YVO_4:20% Yb^{3+},2% Er^{3+} product, aqueous solutions of YCl_3, $YbCl_3$ and $ErCl_3$ were mixed together in a molar ratio 0.78 : 0.2 : 0.02, *i.e.* 3.478 mL of 0.5 M YCl_3, 0.892 mL of 0.5 M $YbCl_3$ and 0.089 mL of 0.5 M $ErCl_3$. Subsequently, 10 mL of water was admixed to the solution of Ln^{3+} ions. Next, 0.5 g of PEG 6000 (anti-agglomeration agent) was added and dissolved in the as-prepared solution. A second solution was prepared by dissolving 0.2607 g of NH_4VO_3 in 20 mL of water. Aqueous sodium hydroxide solution was added to the solution of ammonium metavanadate in a molar ratio of 1 : 1 (0.0892 g of NaOH in 15 mL of water). These solutions were heated up to 343 K to obtain transparent mixtures. The solution containing vanadate ions was added dropwise to the continuously stirred solution of Ln^{3+}. Then water (up to 40 mL volume) was added to the obtained solution, and using 1.5 M solution of NaOH, the pH of the system was adjusted to ≈10. The entire mixture was then transferred into a Teflon-lined vessel, and hydrothermally treated in an autoclave (18 h, 453 K). After that, the obtained white precipitate was dispersed in ethanol and water, and several times centrifuged in order to purify the final product. The obtained product YVO_4:Yb^{3+},Er^{3+} was dried in an oven at 358 K for 15 h, and subsequently the sample was ground in an agate mortar. Afterwards, to improve the crystallinity and luminescence of the material, the sample was calcined in an oven for 4 h at 673 K. After calcination, the product was ground in an agate mortar once again.

Characterization

Powder X-ray diffraction pattern (XRD) was measured using a Bruker AXS D8 Advance diffractometer in Bragg–Brentano geometry, with Cu Kα radiation (λ = 0.15406 nm). Transmission electron microscopy (TEM) image was taken using a Hitachi HT7700 transmission electron microscope (100 kV accelerating voltage). Emission spectra were measured using an Andor Shamrock 500i spectrograph coupled with a silicon iDus CCD camera as a detector. The sample was excited using a fiber-coupled, solid-state diode pumped (SSDP) laser FC-975-2 W (CNI). The laser power used was adjusted to 100, 200 and 300 mW (≈1 mm spot size), which correspond to the power densities of about 12.7, 25.4 and 38.2 W cm^{-2}. Before the luminescence measurements, the laser power was set low enough to avoid an uncontrolled increase in the sample temperature by local heating of the material with the laser beam (when the intensity ratio of the Er^{3+} TCL bands remained constant, the laser-induced heating effect did not occur).

Results and discussion

Structure and morphology

The recorded XRD pattern of the obtained YVO_4:Yb^{3+},Er^{3+} nanomaterial (Fig. 1a) agrees with the reference pattern from the ICDD database (International Centre for Diffraction Data, card no. 01-082-1968) of tetragonal YVO_4, crystallizing in the *I*41/*amd* space group. The significant broadening of the observed reflexes is associated with the nanocrystallinity of the obtained particles. The TEM image (Fig. 1b) shows that the obtained nanomaterial is composed of irregular agglomerated

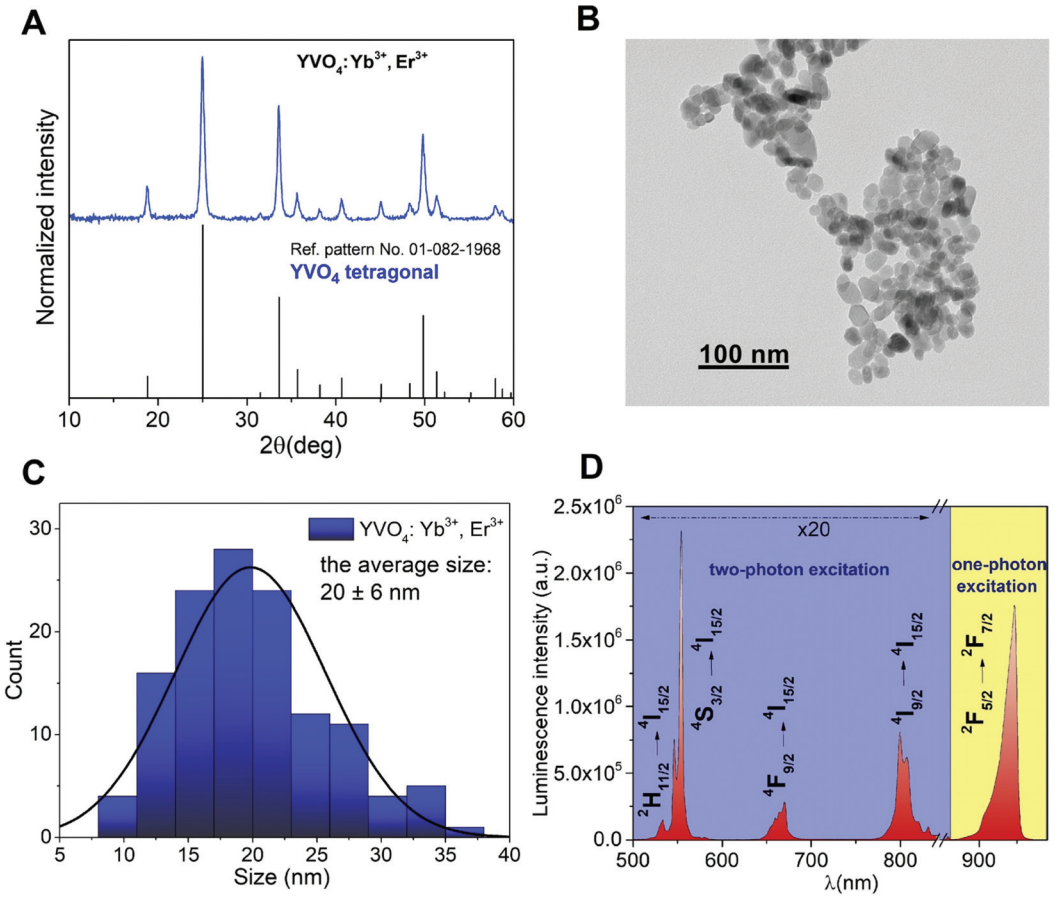

Fig. 1 (a) Powder XRD pattern of YVO_4:Yb^{3+},Er^{3+}; (b) TEM image of the obtained nanomaterial and (c) the corresponding size distribution histogram; and (d) emission spectrum of the obtained product recorded at λ_{ex} = 975 nm and pump power 300 mW.

nanoparticles (NPs), and their average size (long diameter) is about 20 ± 6 nm (Fig. 1c).

Luminescence properties

The emission spectrum was recorded in the range of 500–960 nm (Fig. 1d; λ_{ex} = 975 nm). The nanomaterial prepared shows a very intense green up-conversion (anti-Stokes) luminescence, visible to the naked eye. The emission spectrum consists of 4 narrow, sharp bands from Er^{3+}: $^2H_{11/2} \rightarrow {}^4I_{15/2}$ (532 nm), $^4S_{3/2} \rightarrow {}^4I_{15/2}$ (550 nm), $^4F_{9/2} \rightarrow {}^4I_{15/2}$ (664 nm) and $^4I_{9/2} \rightarrow {}^4I_{15/2}$ (805 nm) associated with their *4f*–*4f* radiative transitions, and one band derived from Yb^{3+}: $^2F_{5/2} \rightarrow {}^2F_{7/2}$ (940 nm), which is partially cut off by the filter used during the measurements (short pass 950 nm). Please note that the filter used has a negligible effect on the rate of change of the relative intensity ratios of the Yb^{3+}/Er^{3+} bands as a function of temperature.[21] The optical characteristics of the 950 nm short pass filter is included in the ESI (Fig. S1†). The Er^{3+} bands located around 664 and 805 nm, as well as the Yb^{3+} band located around 940 nm are in the 1st biological window spectral range. This is very important for the application of a luminescent nanothermometer in biological research. Fig. 2 shows the energy level diagram for the obtained nanomaterial (YVO_4: Yb^{3+},Er^{3+}), taking into account the main energy transfer processes, up-conversion luminescence and thermalization of states.

In order to investigate the influence of temperature on the spectroscopic properties of the obtained nanomaterial, its emission spectra were collected as a function of increasing temperature, in the range of 293–453 K (Fig. 3; λ_{ex} = 975 nm). The measurements were carried out using different values of the laser power (100, 200 and 300 mW), in order to investigate the effect of the pump power on the thermometric properties of the material, *i.e.* performance of the luminescent thermometer. As the temperature increases, a significant decrease in the intensity of the band located around 550 nm (Er^{3+}: $^4S_{3/2} \rightarrow {}^4I_{15/2}$) is observed, as a result of thermal quenching and thermalization processes. Intensity of the Er^{3+} bands located around 532, 664 and 805 nm negligibly change or slightly increase with increasing temperature. These effects can be clearly seen in the non-normalized spectra (Fig. S2†) and in the plots presenting the integrated up-conversion luminescence intensities as a function of temperature (Fig. S3†). The Er^{3+} bands located around 532 and 550 nm ($^2H_{11/2} \rightarrow {}^4I_{15/2}$ and

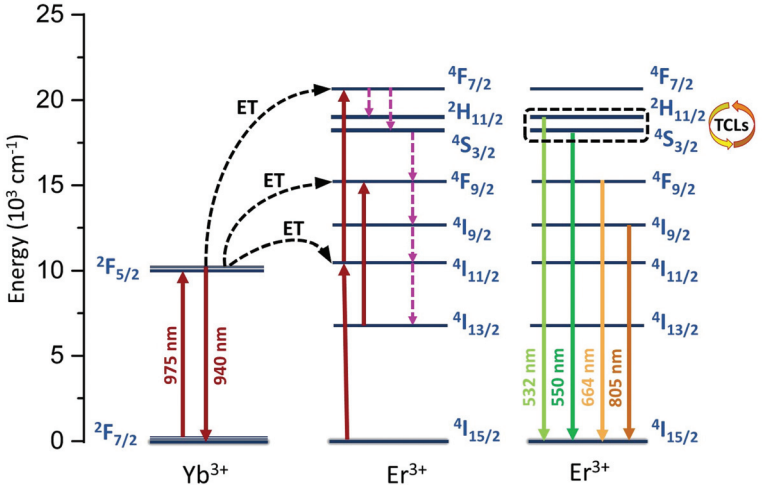

Fig. 2 Energy level diagram showing schematically the possible radiative and non-radiative processes in the YVO_4:Yb^{3+},Er^{3+} system.

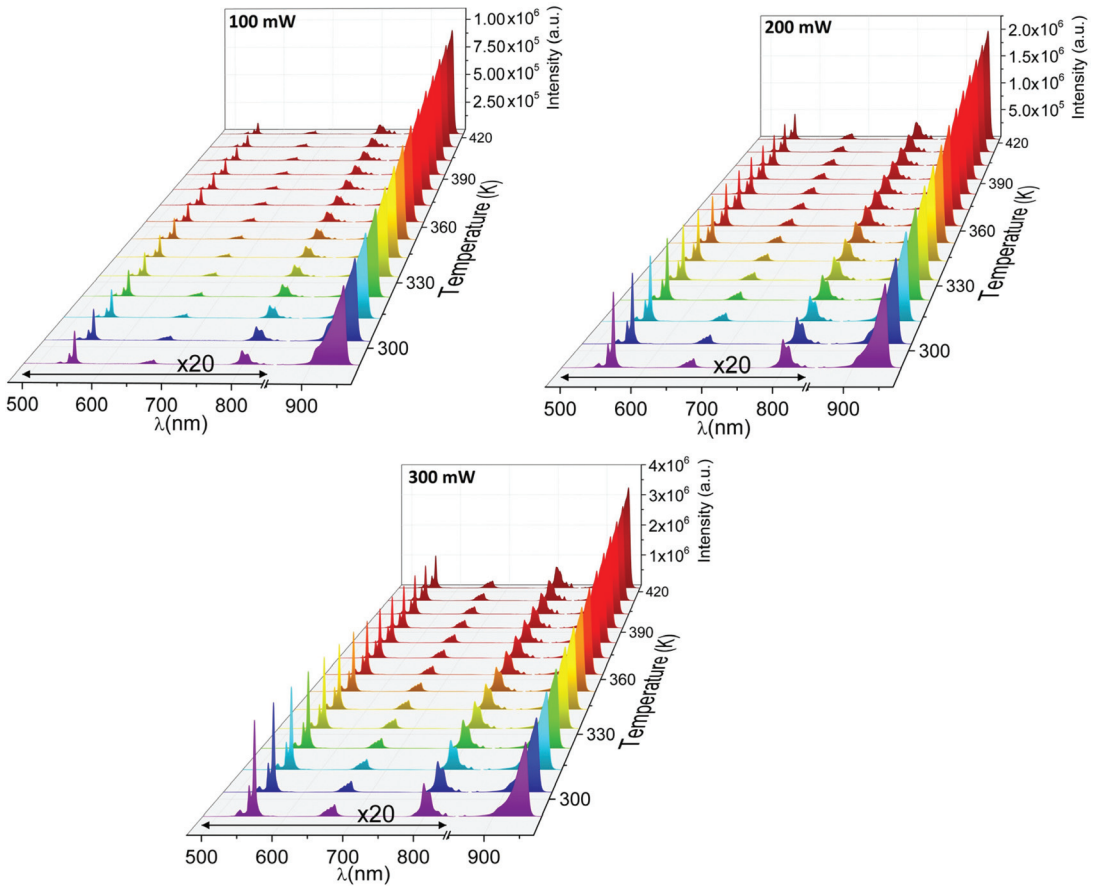

Fig. 3 Emission spectra of the synthesized YVO_4:Yb^{3+},Er^{3+} NPs measured at increasing temperature values and with different laser power (100, 200 and 300 mW); λ_{ex} = 975 nm.

$^4S_{3/2} \rightarrow {}^4I_{15/2}$) are thermally coupled, and the energy difference between these levels is approximately 603 cm^{-1} (derived from the Boltzmann distribution). This is why, the significant, relative increase of the 532 nm band intensity, with respect to the 550 nm band, is due to the thermalization processes between the TCLs of Er^{3+} ($^2H_{11/2}$ and $^4S_{3/2}$), which can be clearly

observed in the normalized spectra (Fig. S4†). These thermalization processes conform the Boltzmann-type distribution:

$$\mathrm{LIR} \equiv \frac{I_2}{I_1} = B \exp\left(-\frac{\Delta E}{k_B T}\right) \quad (1)$$

where LIR is the luminescence intensity ratio of the higher energy (I_2; 532 nm) and lower energy (I_1; 550 nm) bands; ΔE is the energy separation between the barycenters I_2 and I_1; k_B is the Boltzmann constant; T is the absolute temperature; and B is a constant, which depends on the rates of total spontaneous emission, state degeneracies, the branching ratio of the transitions with respect to the ground state, and transition angular frequencies.[30] At the same time, the intensity of the Yb^{3+} band around 940 nm (Yb^{3+}: $^2F_{5/2} \rightarrow {}^2F_{7/2}$) increases with temperature elevation. This is because the band originates from the phonon-assisted transition of Yb^{3+}, which may be enhanced with temperature.[8,21,24]

It should be emphasized that the changes in the pump (laser) power have a significant impact on the absolute intensity of the emission bands, as well as their relative intensities (in the case of the non-TCL ones), especially for the luminescence intensity ratios of Yb^{3+}/Er^{3+}. The band around 940 nm corresponds to the one-photon transition $^2F_{5/2} \rightarrow {}^2F_{7/2}$ (see Fig. S5,† showing the determined number of photons participating in the observed transitions), *i.e.* conventional down-shifting emission. So, even at a relatively low laser power (*i.e.* 100 mW), this transition is intense and clearly visible. On the other hand, in the case of the two-photon transitions coming from Er^{3+} (non-linear, up-conversion luminescence; Fig. S5†), the change of the laser power has a huge impact on the intensity of these bands. Together with decreasing laser power, the signal-to-noise ratio decreases significantly for the up-conversion emission, and the data quality deteriorates markedly. This is why, the change of the pump power influences the determined thermometric parameters associated with non-TCLs, *i.e.* LIRs of Yb^{3+}/Er^{3+}, but it does not affect Er^{3+} TCLs, *i.e.* LIR 532/550 nm. The LIR values for Er^{3+} TCLs, *i.e.* 532/550 nm, were correlated with temperature applying eqn (1) (Fig. 4), whereas the LIRs corresponding to the non-TCLs, *i.e.* 940/550 and 940/805 nm, were successfully correlated with temperature applying second-order polynomial fits (Fig. 5 and 6). In each case, the LIR parameter increases monotonously with increasing temperature. The use of simple polynomial fits (empirical functions) was motivated by the absence of an appropriate physical model, rationalizing the monitored changes of the LIR parameters (non-TCLs) with temperature. Details for all fits, *i.e.* values of the fitting parameters, are given in Table 1.

In order to investigate the performance of any nanothermometer, it is necessary to determine parameters such as: absolute sensitivity, relative sensitivity and temperature resolution. The absolute sensitivity (S_A) was calculated based on eqn (2). This parameter is usually expressed in K^{-1}.

$$S_A = \frac{d\mathrm{LIR}}{dT} \quad (2)$$

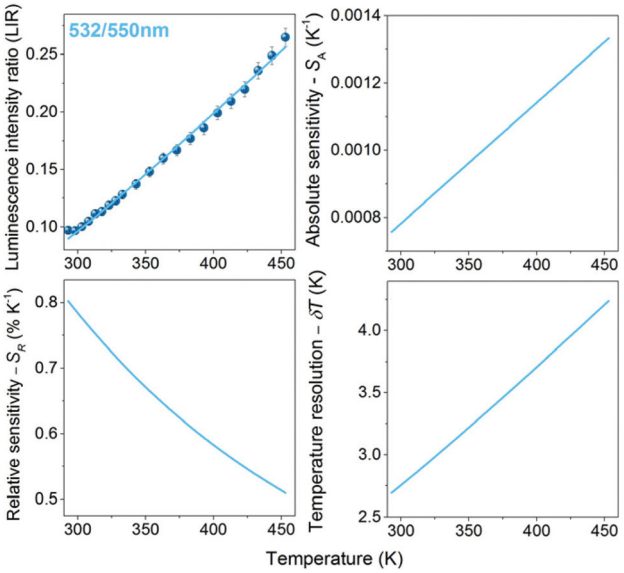

Fig. 4 Luminescence intensity ratios, the corresponding absolute sensitivity (S_A), relative sensitivity (S_R) and temperature resolution (δT) determined for Er^{3+} TCLs (532/550 nm), for the synthesized YVO_4:Yb^{3+},Er^{3+} NPs, measured with laser power 300 mW; λ_{ex} = 975 nm.

Another very important parameter is the relative temperature sensitivity (S_R; eqn (3)).

$$S_R = 100\% \times \frac{d\mathrm{LIR}}{dT}\frac{1}{\mathrm{LIR}} \quad (3)$$

This parameter, *i.e.* S_R, shows how the analyzed thermometric parameter (LIR) changes per 1 K (expressed in % K^{-1}), and it can be used to compare the performance of different optical thermometers.

Based on eqn (4), the temperature resolutions (δT) were also determined.

$$\delta T = \frac{1}{S_R}\frac{\delta\mathrm{LIR}}{\mathrm{LIR}} \quad (4)$$

We have added a more detailed explanation of the temperature resolution parameter δT, and have provided derivation of the corresponding equation in the ESI† file. It is worth mentioning that δLIR is the uncertainty of the LIR parameter determination, which is calculated from eqn (5).

$$\delta\mathrm{LIR} = \mathrm{LIR} \times \sqrt{\left(\frac{\delta I_1}{I_1}\right)^2 + \left(\frac{\delta I_2}{I_2}\right)^2} \quad (5)$$

where $\delta I_{1,2}$ are the intensities of the noise (baseline fluctuations) and $I_{1,2}$ are the signal (band) intensities. The determined S_A, S_R and δT as function of temperature, together with the corresponding LIR values are compared in Fig. 4–6 (Er^{3+} TCL 532/550 nm – Fig. 4; Yb^{3+}/Er^{3+} non-TCLs 940/550 nm and 940/805 nm – Fig. 5 and 6, respectively). Please note that the LIR, S_A and S_R parameters for the TCLs of Er^{3+} are independent (constant) of the pump power used, so Fig. 4 shows the results only for the highest applied laser power, *i.e.* 300 mW

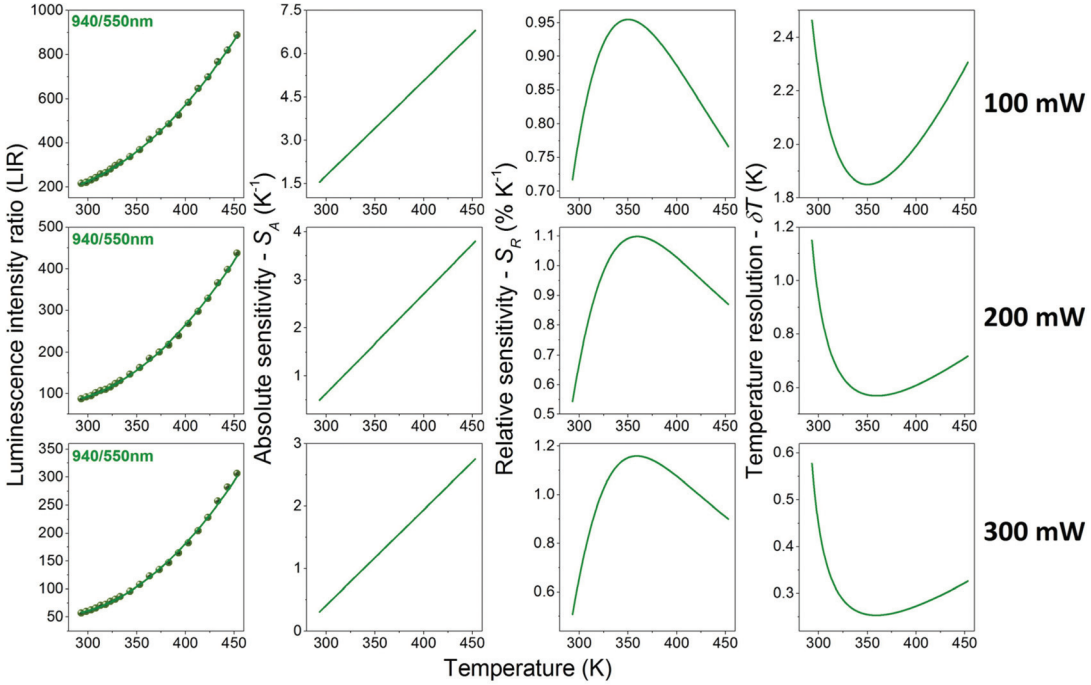

Fig. 5 Luminescence intensity ratios, the corresponding absolute sensitivities (S_A), relative sensitivities (S_R) and temperature resolutions (δT) determined for Yb^{3+}/Er^{3+} (940/550 nm) non-TCLs of the synthesized YVO_4:Yb^{3+},Er^{3+} NPs, measured with different laser power values (100, 200 and 300 mW); λ_{ex} = 975 nm.

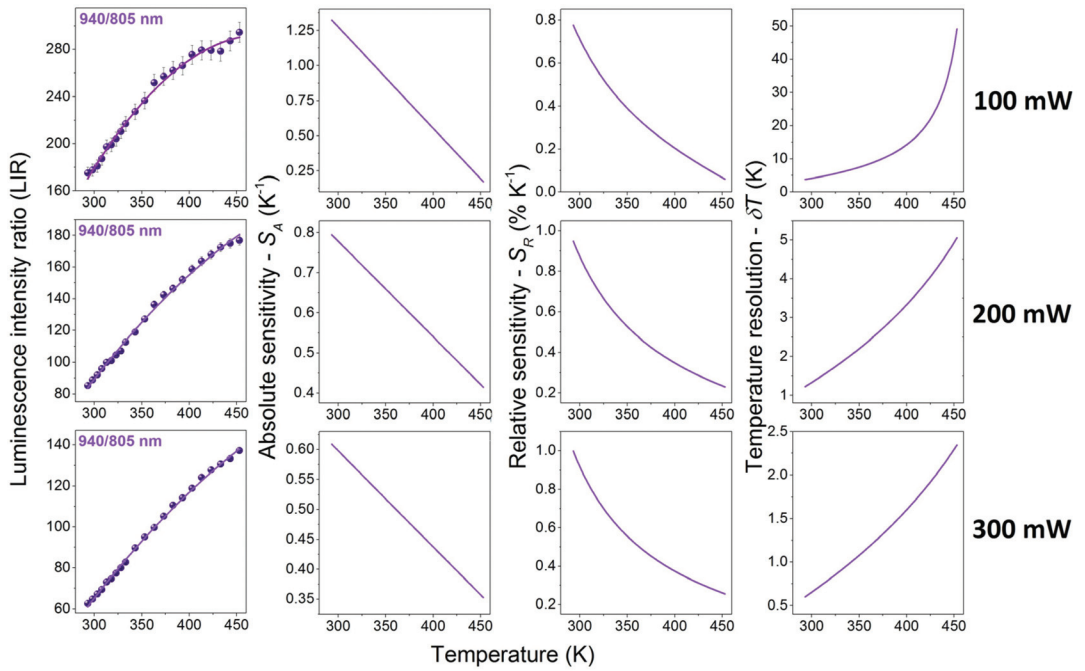

Fig. 6 Luminescence intensity ratios, the corresponding absolute sensitivity (S_A), relative sensitivities (S_R) and temperature resolution (δT) determined for Yb^{3+}/Er^{3+} (940/805 nm) non-TCLs of the synthesized YVO_4:Yb^{3+},Er^{3+} NPs, measured with different laser power values (100, 200 and 300 mW); λ_{ex} = 975 nm.

(the maximum power at which we did not observe laser-induced heating of the sample). On the other hand, Fig. 5 and 6 show the data for the non-TCLs of Yb^{3+}/Er^{3+}, for three different values of the laser power, *i.e.* 100, 200 and 300 mW, because in this case all measured parameters depend on the pump power used.

Table 1 Comparison of the determined $S_{R\ max}$ and δT for different laser power values and the corresponding LIR

LIR (nm)	Transitions	R^2	Equation	Laser power (mW)	$S_{R\ max}$ (% K^{-1})	δT (K)
532/550	Er^{3+}: $^2H_{11/2} \rightarrow {}^4I_{15/2}$/$Er^{3+}$: $^4S_{3/2} \rightarrow {}^4I_{15/2}$	0.998	$1.74 \exp(-603.2/k_BT)$	300	0.80	2.69
940/550	Yb^{3+}: $^2F_{5/2} \rightarrow {}^2F_{7/2}$/$Er^{3+}$: $^4S_{3/2} \rightarrow {}^4I_{15/2}$	0.999	$6.86 \times 10^{-3}T^2 - 3.60T + 522.8$	100	0.95	1.85
		0.998		200	1.10	0.57
		0.999		300	1.16	0.25
940/805	$Yb^{3+}(^2F_{5/2} \rightarrow {}^2F_{7/2})$/$Er^{3+}$: $^4I_{9/2} \rightarrow {}^4I_{15/2}$	0.991	$-6.77 \times 10^{-4}T^2 + 0.99\ T - 170.13$	100	0.78	3.75
		0.996		200	0.95	1.22
		0.997		300	1.00	0.60

As mentioned above and clearly seen in Fig. 5 and 6, the applied laser power has a significant influence on the values of the band intensity ratios, temperature sensitivities and resolutions, when using the LIRs of the non-TCLs as thermometric parameters. For the analyzed band intensity ratios, *i.e.* 940/550 and 940/805 nm, corresponding to the non-TCLs of Yb^{3+}/Er^{3+}, the increase in the laser power results in decreasing LIR, S_A and δT, and increasing S_R values. The most important of these are the increase of the relative sensitivity (higher S_R) and the improvement of temperature resolution (lower δT). Together with increasing laser power from 100 to 300 mW, the maximal relative sensitivity ($S_{R\ max}$) values increase from 0.78 to 1.00 for the LIR 940/805 nm and from 0.95 to 1.16 for the LIR 940/550 nm. In contrast, the temperature resolutions (which depend on signal intensity and S_R value) are about 6–7 times better than those at 100 mW, *e.g.* δT decrease from 3.75 to 0.60 for the LIR 940/805 nm and from 1.85 to 0.25 for the LIR 940/550 nm. It is worth noting that the resulting temperature sensitivities and resolutions corresponding to Er^{3+} TCLs (532/550 nm), determined at the highest applied laser power (300 mW), are worse than the ones for Yb^{3+}/Er^{3+} non-TCLs (see Table 1).

Conclusions

In this paper, we demonstrate how the applied laser power may influence the thermometric parameters and sensing performance, which are crucial for luminescence thermometry applications. The developed nanothermometer is based on the YVO_4:Yb^{3+},Er^{3+} NPs (≈20 nm), synthesized using the hydrothermal method and subsequent calcination. The nanomaterial shows green up-conversion (anti-Stokes) luminescence of Er^{3+}, clearly visible to the naked eye, under NIR laser excitation, at 975 nm. The temperature experiments were carried out in the range of 293–453 K, using different values of the laser power, namely 100, 200 and 300 mW. As the temperature increases, the intensity of the band derived from Er^{3+} ions located around 550 nm ($^4S_{3/2} \rightarrow {}^4I_{15/2}$) decreases significantly, whereas the intensity of the Yb^{3+} band >900 nm ($^2F_{5/2} \rightarrow {}^2F_{7/2}$) increases with temperature elevation. Hence, as thermometric parameters we used and compared the LIR of Er^{3+} (532/550 nm) and the LIRs of the mentioned Yb^{3+}/Er^{3+} (940/550 and 940/805 nm) bands, corresponding to their TCLs and non-TCLs. It was observed that using non-TCLs for ratiometric temperature sensing, the selected pump (laser) power has a significant impact on the values of the corresponding thermometric parameters, as well as on the determined sensitivities and resolutions (S_R increases and δT decreases with increasing laser power). In other words, in the case of luminescent thermometers exhibiting non-linear phenomena (*e.g.* up-conversion emission), and using the LIR of the bands originating from the transitions with a different number of photons participating in the relevant radiative processes, change of the laser power may significantly affect the determined thermometric parameter values, and performance of the sensor.

Conflicts of interest

The authors declare no conflict of interest.

Acknowledgements

This work was supported by the Polish National Science Centre (grant no. 2018/31/N/ST4/00684).

References

1 M. Kamimura, T. Matsumoto, S. Suyari, M. Umezawa and K. Soga, *J. Mater. Chem. B*, 2017, **5**, 1917–1925.
2 S. K. Singh, K. Kumar and S. B. Rai, *Sens. Actuators, A*, 2009, **149**, 16–20.
3 B. Dong, D. P. Liu, X. J. Wang, T. Yang, S. M. Miao and C. R. Li, *Appl. Phys. Lett.*, 2007, **90**, 3–6.
4 R. G. Geitenbeek, P. T. Prins, W. Albrecht, A. Van Blaaderen, B. M. Weckhuysen and A. Meijerink, *J. Phys. Chem. C*, 2017, **121**, 3503–3510.
5 H. Suo, F. Hu, X. Zhao, Z. Zhang, T. Li, C. Duan, M. Yin and C. Guo, *J. Mater. Chem. C*, 2017, **5**, 1501–1507.
6 A. A. Kalinichev, M. A. Kurochkin, E. V. Golyeva, A. V. Kurochkin, E. Lähderanta, M. D. Mikhailov and I. E. Kolesnikov, *J. Lumin.*, 2018, **195**, 61–66.
7 S. Jiang, P. Zeng, L. Liao, S. Tian, H. Guo, Y. Chen, C. Duan and M. Yin, *J. Alloys Compd.*, 2014, **617**, 538–541.
8 N. Stopikowska, M. Runowski, P. Woźny, S. Goderski and S. Lis, *J. Lumin.*, 2020, **228**, 117643.

9 L. Marciniak, A. Bednarkiewicz, M. Stefanski, R. Tomala, D. Hreniak and W. Strek, *Phys. Chem. Chem. Phys.*, 2015, **17**, 24315–24321.
10 M. Runowski, N. Stopikowska and S. Lis, *Dalton Trans.*, 2020, **49**, 2129–2137.
11 A. Nadort, J. Zhao and E. M. Goldys, *Nanoscale*, 2016, **8**, 13099–13130.
12 M. Runowski, in *Handbook of Nanomaterials in Analytical Chemistry*, Elsevier, 2020, pp. 227–273.
13 D. Jaque and F. Vetrone, *Nanoscale*, 2012, **4**, 4301–4326.
14 T. Xia, Y. Cui, Y. Yang and G. Qian, *J. Mater. Chem. C*, 2017, **5**, 5044–5047.
15 A. Benayas, *Near Infrared-Emitting Nanoparticles for Biomedical Applications*, 2020.
16 M. A. Hernández-Rodríguez, A. D. Lozano-Gorrín, I. R. Martín, U. R. Rodríguez-Mendoza and V. Lavín, *Sens. Actuators, B*, 2018, **255**, 970–976.
17 Y. Tian, Y. Tian, P. Huang, L. Wang, Q. Shi and C. Cui, *Chem. Eng. J.*, 2016, **297**, 26–34.
18 L. Marciniak, A. Bednarkiewicz, J. Drabik, K. Trejgis and W. Strek, *Phys. Chem. Chem. Phys.*, 2017, **19**, 7343–7351.
19 W. Xu, Q. Song, L. Zheng, Z. Zhang and W. Cao, *Opt. Lett.*, 2014, **39**, 4635.
20 M. Runowski, N. Stopikowska, D. Szeremeta, S. Goderski, M. Skwierczyńska and S. Lis, *ACS Appl. Mater. Interfaces*, 2019, **11**, 13389–13396.
21 M. Runowski, S. Goderski, D. Przybylska, T. Grzyb, S. Lis and I. R. Martín, *ACS Appl. Nano Mater.*, 2020, **3**, 6406–6415.
22 L. Labrador-Páez, M. Pedroni, A. Speghini, J. García-Solé, P. Haro-González and D. Jaque, *Nanoscale*, 2018, **10**, 22319–22328.
23 I. K. van Ravenhorst, R. G. Geitenbeek, M. J. van der Eerden, J. Tijn van Omme, H. H. Peréz Garza, F. Meirer, A. Meijerink and B. M. Weckhuysen, *ChemCatChem*, 2019, **11**, 5505–5512.
24 T. Bai and N. Gu, *Small*, 2016, **12**, 4590–4610.
25 H. Pinkerton, M. James and A. Jones, *J. Volcanol. Geotherm. Res.*, 2002, **113**, 159–176.
26 C. D. S. Brites, P. P. Lima, N. J. O. Silva, A. Millán, V. S. Amaral, F. Palacio and L. D. Carlos, *Nanoscale*, 2012, **4**, 4799–4829.
27 M. Runowski, A. Shyichuk, A. Tymiński, T. Grzyb, V. Lavín and S. Lis, *ACS Appl. Mater. Interfaces*, 2018, **10**, 17269–17279.
28 S. F. León-Luis, U. R. Rodríguez-Mendoza, E. Lalla and V. Lavín, *Sens. Actuators, B*, 2011, **158**, 208–213.
29 M. D. Dramićanin, *J. Appl. Phys.*, 2020, **128**, 040902.
30 C. D. S. Brites, A. Millán and L. D. Carlos, *Handb. Phys. Chem. Rare Earths*, 2016, **49**, 339–427.
31 K. Mukhuti, V. N. K. B. Adusumalli, K. Raj, R. B. Bansal and V. Mahalingam, *J. Lumin.*, 2020, **227**, 117542.
32 R. G. Geitenbeek, H. W. De Wijn and A. Meijerink, *Phys. Rev. Appl.*, 2018, **10**, 064006.
33 L. Li, F. Qin, L. Li, H. Gao and Z. Zhang, *J. Mater. Chem. C*, 2019, **7**, 7378–7385.
34 C. D. S. Brites, K. Fiaczyk, J. F. C. B. Ramalho, M. Sójka, L. D. Carlos and E. Zych, *Adv. Opt. Mater.*, 2018, **6**, 1–5.
35 E. C. Ximendes, U. Rocha, T. O. Sales, N. Fernández, F. Sanz-Rodríguez, I. R. Martín, C. Jacinto and D. Jaque, *Adv. Funct. Mater.*, 2017, **27**, 1–10.
36 M. Runowski, P. Woźny, N. Stopikowska, I. R. Martín, V. Lavín and S. Lis, *ACS Appl. Mater. Interfaces*, 2020, **12**, 43933–43941.
37 C. Wang, Y. Jin, L. Yuan, H. Wu, G. Ju, Z. Li, D. Liu, Y. Lv, L. Chen and Y. Hu, *Chem. Eng. J.*, 2019, **374**, 992–1004.